Journal of Alloys and Compounds 523 (2012) 88–93

Contents lists available at SciVerse ScienceDirect

Journal of Alloys and Compounds

journal homepage: www.elsevier.com/locate/jallcom

Self-consistent simulation of carrier confinement characteristics in $(Al_yGa_{1-y}N/AlN)SLs/GaN/(In_xGa_{1-x}N/GaN)MQW/GaN$ heterostructures

Jieqin Ding[a,*], Xiaoliang Wang[a,b,c], Hongling Xiao[a,b], Cuimei Wang[a,b], Haibo Yin[a,b], Hong Chen[a,b], Chun Feng[a,b], Lijuan Jiang[a,b]

[a] Materials Science Center, Institute of Semiconductors, Chinese Academy of Sciences, P.O. Box 912, Beijing 100083, PR China
[b] Key Lab of Semiconductor Materials Science, Institute of Semiconductors, Chinese Academy of Sciences, P.O. Box 912, Beijing 100083, PR China
[c] ISCAS-XJTU Joint Laboratory of Functional Materials and Devices for Informatics, PR China

ARTICLE INFO

Article history:
Received 18 October 2011
Received in revised form 9 January 2012
Accepted 15 January 2012
Available online 8 February 2012

PACS:
73.61.Ey
73.40.Kp
02.60.Cb

Keywords:
Heterojunctions
Nitride materials
Semiconductors
Electronic properties

ABSTRACT

We present calculations of carrier confinement characteristics in $(Al_yGa_{1-y}N/AlN)SLs/GaN/(In_xGa_{1-x}N/GaN)MQW/GaN$ heterojunction structure in the presence of spontaneous and piezoelectrically induced polarization effects. The calculations were made using a self-consistent solution of the Schrödinger, Poisson, potential and charge balance equations. An optimization of $In_xGa_{1-x}N/GaN$ multiquantum-well (MQW) was made firstly including thickness of GaN channel, InGaN, and indium composition of $In_xGa_{1-x}N$ in order to increase carrier density and mobility, and the influence of pairs of AlGaN/AlN superlattices (SLs) and InGaN/GaN MQWs on structure was discussed. Theoretical calculations clearly indicate that the two-dimensional electron gas (2DEG) sheet carrier density in designed heterostructure is greatly increased due to the enhancing of carrier confinement compared to those in conventional AlGaN/GaN one at the similar Al composition. Furthermore, the calculated carrier distribution shows that carrier mobility will be improved by reducing interface roughness and alloy disorder scattering in designed heterostructure.

1. Introduction

AlGaN/GaN high electron mobility transistors (HEMT) are believed to be much promising for application to high power and high frequency devices [1–7]. Unlike many other semiconductors, GaN-based material has both a spontaneous and a piezoelectric component, both of which determine the total polarization. The abrupt change of the polarization causes a bound sheet charge density at the AlGaN/GaN interface, and for Ga (Al) face nitrides, free electrons are attracted to compensate this charge by forming a 2DEG in the GaN close to the interface. Owing to having large lattice mismatch and piezoelectric coefficients between AlGaN (AlN) and GaN, a polarization electric field, which inducing a high sheet charge density in the order of 10^{13} cm^{-2}, is produced at the AlGaN (AlN)/GaN heterojunction [8,9].

Carrier confinement has significant impact on 2DEG density and its mobility in HEMT structures. For the barrier layer, excellent carrier confinement characteristics can lower carriers penetrating into barrier, which will reduce interface roughness and alloy disorder scattering leading to high sheet carrier density and mobility [10]. For back-barrier layer, a sharp rise of conduction band can prevent 2DEG leaking to the buffer layer effectively, and suppress current collapse effect, therefore improved pinch-off characteristics for HEMT devices can be achieved [11,12]. Experiments of these attempts have been made by several researchers. Micovic et al. [13] demonstrated an AlGaN/GaN/AlGaN double-heterojunction HEMT with improved buffer isolation by using an AlGaN buffer layer with an Al composition of 4%. Kawakami et al. [14] have designed a AlGaN/GaN heterostructure using AlN/GaN SLs as barrier layer. Lee et al. [15] have reported AlGaN/GaN HEMT structure based on InGaN/GaN MQW. However, insufficient literature about numerical simulations for investigating the carrier confinement characteristics has been found.

In this paper, we will focus on the investigation of electrical properties of 2DEG in $(Al_yGa_{1-y}N/AlN)SLs/GaN/(In_xGa_{1-x}N/GaN)MQW/GaN$ heterojunction structures by solving one-dimensional Schrödinger and Poisson's equations self-consistently. By analysing the band structure, carrier density, polarization charges distribution, and the relationship between 2DEG distributions and mobility, mechanisms for the improvement of carrier confinement characteristics were discussed by comparing with related AlGaN/GaN structure. The calculation

* Corresponding author. Tel.: +86 10 82304140; fax: +86 10 82304045.
E-mail address: jieqinding@semi.ac.cn (J. Ding).

0925-8388/$ – see front matter © 2012 Elsevier B.V. All rights reserved.
doi:10.1016/j.jallcom.2012.01.073

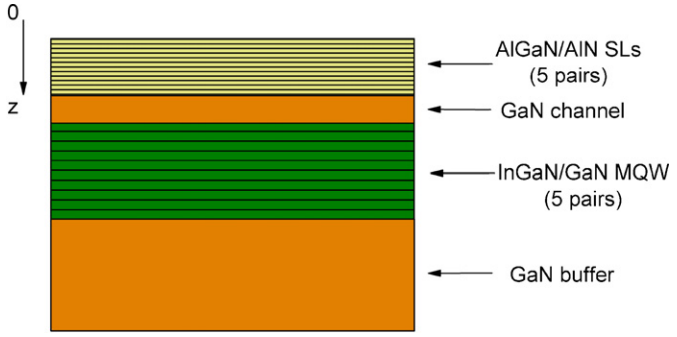

Fig. 1. The schematic of HEMT structure in the calculations.

begins with an optimization of the $In_xGa_{1-x}N$/GaN MQW which including thickness of GaN channel, InGaN, and indium composition of $In_xGa_{1-x}N$ in order to increase carrier density and mobility, Details of the calculation will be described.

2. Device structures and simulation

2.1. Modelling

The general layer sequence of the modeled HEMT structures is shown in Fig. 1. All of the layers are assumed to coherently grown along [0 0 0 1]. The barrier layer is formed by 5 pairs $Al_yGa_{1-y}N$/AlN SLs ($Al_yGa_{1-y}N$ thickness t_{AlGaN}: 1.5 nm, AlN thickness t_{AlN}: 0.5 nm), and the equivalent Al composition χ_{Al} of whole SLs barrier layer is expressed as follows:

$$\chi_{Al} = y\left(\frac{t_{AlGaN}}{t_{AlGaN}+t_{AlN}}\right) + \frac{t_{AlN}}{t_{AlGaN}+t_{AlN}}, \quad (1)$$

where y is Al composition of $Al_yGa_{1-y}N$ in the $Al_yGa_{1-y}N$/AlN SLs, t_{AlGaN} and t_{AlN} is the layer thicknesses of $Al_yGa_{1-y}N$ and AlN, respectively. The back-barrier MQW is formed by 5 pairs $In_xGa_{1-x}N$/GaN, and the indium composition and thickness of $In_xGa_{1-x}N$ will be optimized.

2.2. Simulation

In this calculation, it is supposed that the sheet carriers in the GaN channel come from the surface donors [16,17] and the Fermi level is in the middle of the bandgap at the AlGaN surface under equilibrium conditions because the AlGaN barrier layer is undoped. The spontaneous polarization along the c axis of the wurtzite crystal is directed opposite to the growth direction for GaN and AlN. Due to the nonideality of the structure, the theoretical spontaneous polarization is very large in the nitrides and also increases from GaN to InN and AlN (Table 1). Piezoelectric polarization arises from the strain effect at the AlGaN/GaN interface and the lattice constant mismatch between these two materials.

Table 1
Spontaneous polarization, lattice, piezoelectric, and elastic constants for III–V wurtzite nitrides.

	AlN	GaN	InN
a_0 (Å)	3.112[b]	3.189[b]	3.54[b]
e_{31} (C/m^2)	−0.60[a]	−0.49[a]	−0.57[a]
e_{33} (C/m^2)	1.46[a]	0.73[a]	0.97[a]
c_{13} (GPa)	108[c]	103[c]	92[c]
c_{33} (GPa)	373[c]	405[c]	224[c]
P_{sp} (C/m^2)	−0.08[a]	−0.029[a]	−0.032[a]

[a] Ref. [18].
[b] Ref. [19].
[c] Ref. [8].

Since the surface conditions are not well understood due to the surface oxidation, etc., we use a Schottky-barrier-diode structure in order to compare the related heterostructures at the same condition. We assume the Schottky contact metal is nickel, which the work function is 5.15 eV. The electron affinity of AlN and GaN are 1.9 eV [20] and 3.4 eV [21], respectively. The electron affinity of $Al_yGa_{1-y}N$ could be obtained by Vegard's law. Thus the Schottky-barrier height ϕ_s of metal/$Al_yGa_{1-y}N$ can be expressed as follows:

$$\phi_s = u_{Ni} - u_{Al_yGa_{1-y}N}, \quad (2)$$

where u_{Ni} and $u_{Al_yGa_{1-y}N}$ are the work function of nickel and $Al_yGa_{1-y}N$, respectively. The electron effective masses in GaN and AlN used are 0.22 m_0 and 0.30 m_0, respectively, where m_0 is the free electron mass. The electron effective mass of $Al_yGa_{1-y}N$ is obtained by a linear interpolation between the values for GaN and AlN. We used the values of the polarization induced sheet charge density at the AlGaN/GaN interface, which was reported in Ref. [22]. The method of calculating the fixed polarization charge density at the nitride heterointerface has been discussed in detail [23].

For free electrons, the envelope wave function ψ_i and the ith subband energy E_i are given by the Schrödinger equation

$$\frac{-\hbar^2}{2}\left[\frac{d}{dz}\left(\frac{1}{m^*}\frac{d\psi_i}{dz}\right)\right] + V(z)\psi_i = E_i\psi_i, \quad (3)$$

$$V(z) = V_h(z) + V_p(z) + V_{2D}(z) \quad (4)$$

where m^* is the effective mass of the electrons, $V_h(z)$ is the conduction band edge potential function of heterojunction structure, $V_p(z)$ is the potential induced by polarization charge and $V_{2D}(z)$ is the electronic potential which is related to 2DEG distribution by Poisson's equation,

$$\frac{d}{dz}\left(\varepsilon\frac{d}{dz}V_{2D}(z)\right) = -qN_{2D}(z) \quad (5)$$

Under equilibrium conditions, the distribution of the 2DEG in each subband obeys Fermi statistics, and the distribution of 2DEG is determined by

$$N_{2D}(z) = \sum_i \frac{m^*KT}{\pi\hbar^2}\ln\left[1+\exp\left(\frac{E_f-E_i}{KT}\right)\right]\left|\psi_i(z)\right|^2 \quad (6)$$

where K is the Boltzmann constant and T is the temperature, which is set at 300 K in our calculation. The coupled Schrödinger and Poisson equation is solved self-consistently.

3. Results and discussion

In the simulations, the Al composition of $Al_yGa_{1-y}N$ in $Al_yGa_{1-y}N$/AlN SLs barrier layers is kept at 0.1 (equivalent Al composition χ_{Al} of the whole SLs barrier layers is 0.32), and the thickness of GaN channel, InGaN, and indium composition of InGaN are changed systematically in order to choose proper parameters for electrical properties of the modeled structure, followed by analysis of the band structure, carrier density, polarization charges distributions as well as the relationship between 2DEG distributions and mobility.

3.1. Proper thickness of GaN channel

The calculated conduction band energy diagram of an $(Al_{0.1}Ga_{0.9}N$/AlN)SLs/GaN/$(In_xGa_{1-x}N$/GaN)MQW/GaN HEMT structure with different GaN channel thicknesses is shown in Fig. 2(a). The sheet carrier density of the designed HEMT structure versus GaN channel thickness is shown Fig. 2(b). In these calculations, the InGaN in InGaN/GaN MQW back barrier layer's thickness is taken as 3 nm, and the indium composition is kept at

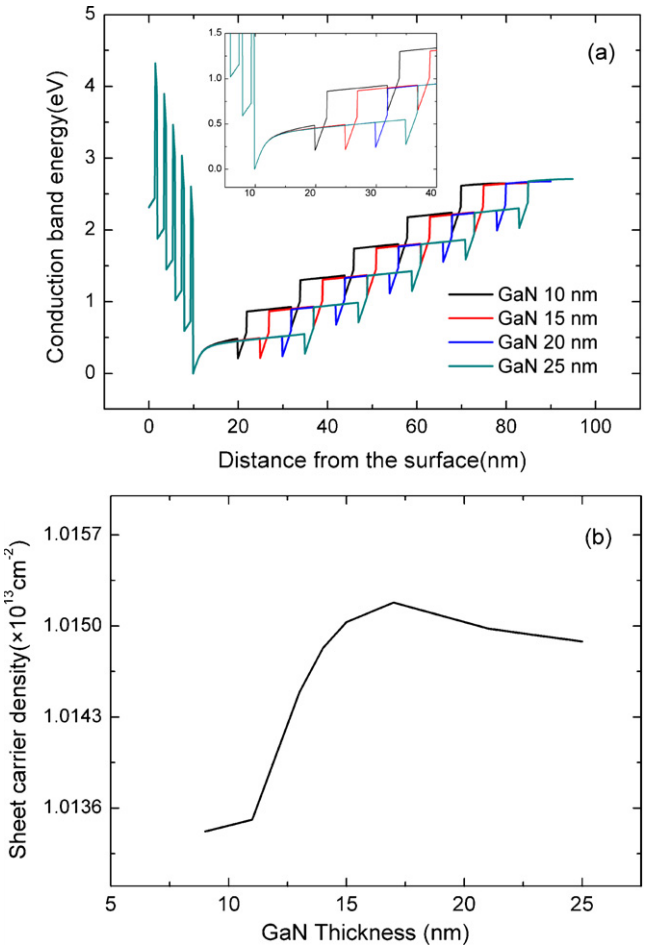

Fig. 2. (a) Calculated conduction band energy diagram of a designed structure with different GaN channel thicknesses. Inset: a closer view of GaN/InGaN region. (b) Sheet carrier density of the designed HEMT structure versus GaN channel thickness.

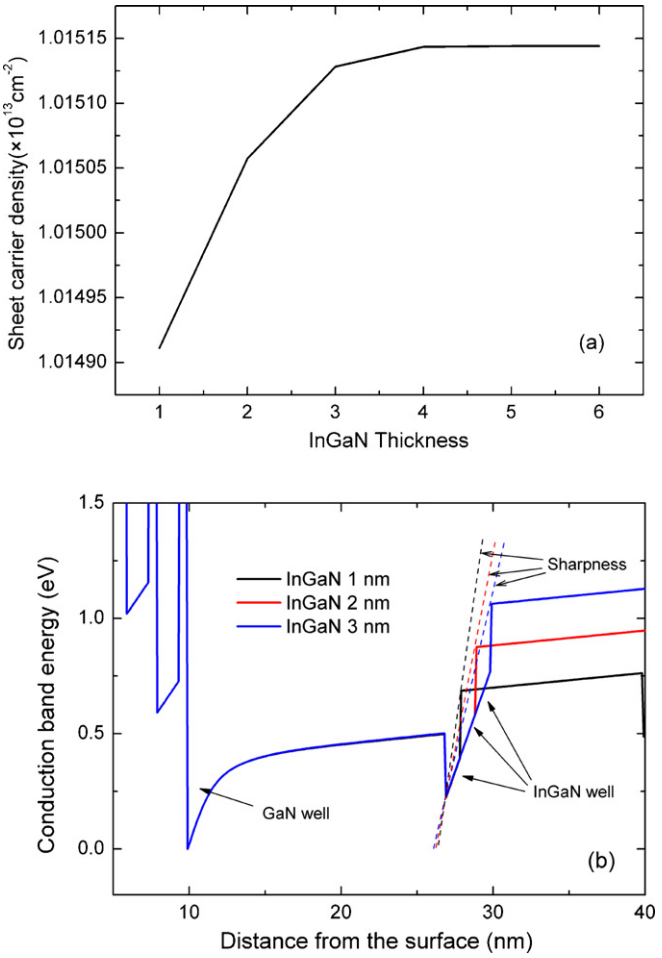

Fig. 3. (a) Calculation of sheet carrier density of the designed HEMT structure versus different InGaN thicknesses. (b) Conduction band diagrams for structures with 1, 2, and 3 nm thick InGaN layer.

0.1. As can be seen that the sheet carrier density increases in large increments up to 17 nm GaN channel thickness, and makes a peak at this value and starts to decrease slowly. Although the change in the sheet carrier density is not very significant, the electron confinement effect of the InGaN/GaN MQW back barrier layer is smaller for higher GaN channel thicknesses. Therefore, a 17 nm thickness value is chosen as the optimum value for GaN channel thickness.

3.2. Optimum thickness of InGaN layer in InGaN/GaN MQWs

As the optimum thickness of GaN channel is 17 nm, in this step, the thickness of InGaN layer is swept from 1 to 6 nm, and the indium composition is kept at 0.1. Fig. 3(a) shows the sheet carrier density of the designed HEMT structure versus different InGaN thicknesses. Fig. 3(b) shows the conduction band diagrams for the structure with 1, 2, and 3 nm thick InGaN layer. It is clear that the sheet carrier density has no considerable change with respect to InGaN thickness, and the potential barrier, formed by InGaN layer's opposite piezoelectric polarization field, increases with increasing the InGaN layer thickness. However, from Fig. 3(b), the conduction band offset at the interface between InGaN-notch and GaN looses its sharpness, as a result, the degree of electron confinement and mobility will decrease. Furthermore, from an experimental point of view, the thickness of InGaN layer should be kept as thin as possible to reduce the risk of indium cluster formation [15]. Considering these factors, we choose 1 nm thickness of InGaN for the following calculations.

3.3. Optimum indium composition of $In_xGa_{1-x}N$

With 17 nm GaN channel and 1 nm InGaN layer, the indium composition of $In_xGa_{1-x}N$ was calculated from 0.05 to 0.20. The indium composition dependence of sheet carrier density of the designed structure is shown in Fig. 4(a), and the conduction band diagrams with varying indium composition are shown in Fig. 4(b). It is clear that the sheet carrier density decreases rapidly with indium composition larger than 0.1, and the InGaN wells are prone to get deeper with greater indium compositions. Nevertheless, experimentally, it was found that the leakage current for greater indium compositions HEMT devices will be large because electrons may spill over from minor channels (formed by opposite piezoelectric polarization in the InGaN layer as opposed to the GaN layer) to the buffer layer [15]. Therefore, the indium composition of InGaN is proposed at 0.1. However, it should be noted that keeping this proposed value is problematic because it is difficult to precisely control the indium composition of the InGaN layer in growth processes [24].

3.4. Influence of the pairs of AlGaN/AlN SLs and InGaN/GaN MQWs on the structure

The sheet carrier density with different pairs of AlGaN/AlN SLs and InGaN/GaN MQWs is shown in Fig. 5. It is seen that there is a threshold pair number below which the 2DEG is not formed. According to the surface state theory [16], for very thin barriers (e.g. one or two pairs of AlGaN/AlN SLs), the ionization energy E_d falls

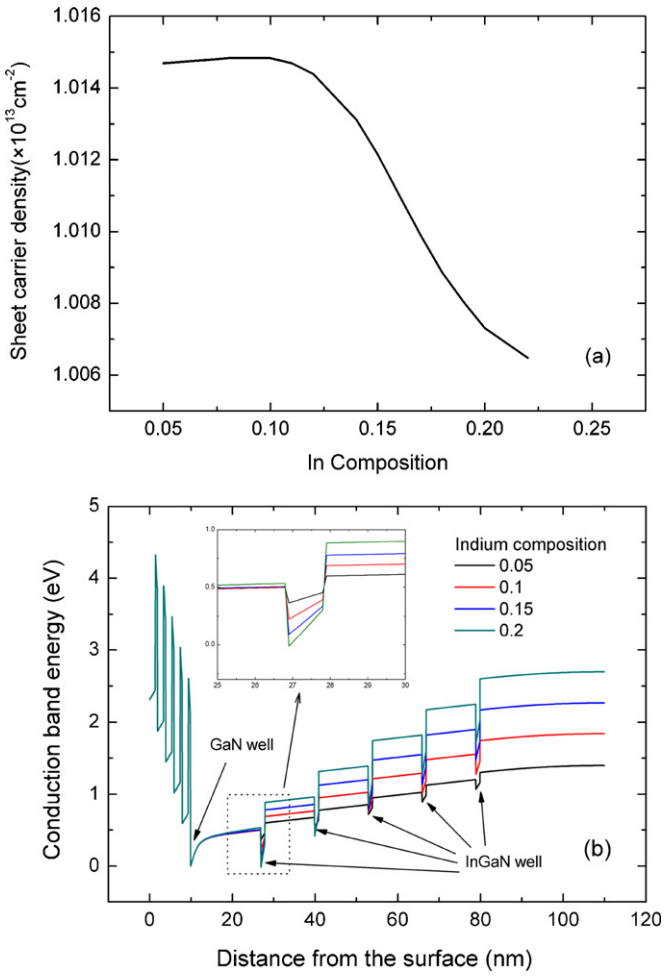

Fig. 4. (a) Calculation of indium composition dependence of sheet carrier density of the designed structure. (b) Conduction band diagrams with varying indium composition. Inset: a closer view of InGaN well.

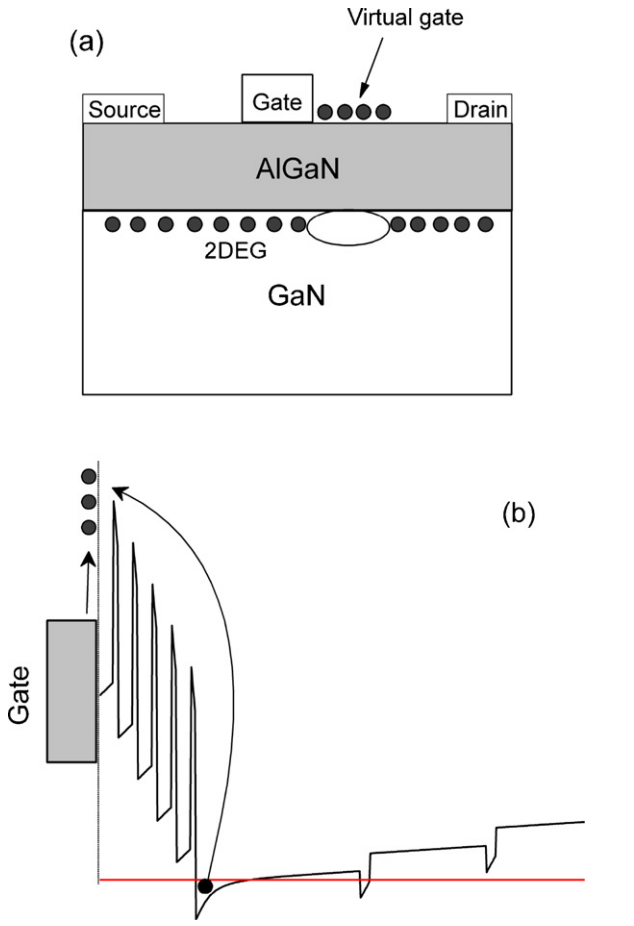

Fig. 6. (a) Occupied AlGaN surface states forming a negatively biased virtual gate and depleting 2DEG. (b) Schematics of possible charging paths to charge AlGaN surface states for ultra-thin barrier.

below Fermi level E_f, preventing surface state ionization. As the barrier thickness is increased (three pairs or more), E_d approaches E_f, enabling more and more surface states to be ionized and leading a sharp increase of 2DEG density. Furthermore, from the point of view of device processes, reducing the gate length L_g is a fundamental technique for FETs to enhance high frequency characteristics, the ultra-thin barrier (no more than 10 nm) used here can derive the maximum benefit from the L_g reduction by keeping high aspect ratio between L_g and barrier thickness. However, previous studies have proposed that AlGaN surface states upon accepting electrons form a negative surface potential, which is, in effect, equivalent to negatively charging an imaginary virtual gate on the surface [25,26]. As it is suggested in Fig. 6(a), this negative virtual gate partially depletes the channel of electrons and extends the depletion region. Within normal thick AlGaN barrier (generally 20–30 nm), electrons in GaN channel gain large kinetic energy in the high electric field region around the gate metal edge. As a result, a fraction of electron population is able to overcome the AlGaN barrier, but these field-accelerated hot electrons may lose their kinetic energy through relaxation by emitting phonons on the way to the surface and be pulled back to the 2DEG channel by the reverse polarization field in this thick AlGaN barrier, thus the AlGaN surface states accepting electrons from 2DEG channel is improbable. In contrast, for the ultra-thin AlGaN/AlN barrier, it is reasonable to suspect that the AlGaN surface states can be charged not only by injected electrons from the gate metal but also by these hot electrons since there is a reduced possibility of energy relaxation due to its barrier thickness, as illustrated in Fig. 6(b). Thus the 2DEG channel offers an additional path to charge the AlGaN surface states, the detrimental virtual gate effect is therefore enhanced. For InGaN/GaN MQWs, it is seen from Fig. 5 that the sheet carrier density keeps unaffected until the pairs of InGaN/GaN MQWs is increased to five. It should be noted that the increase in pairs of InGaN/GaN MQWs makes an

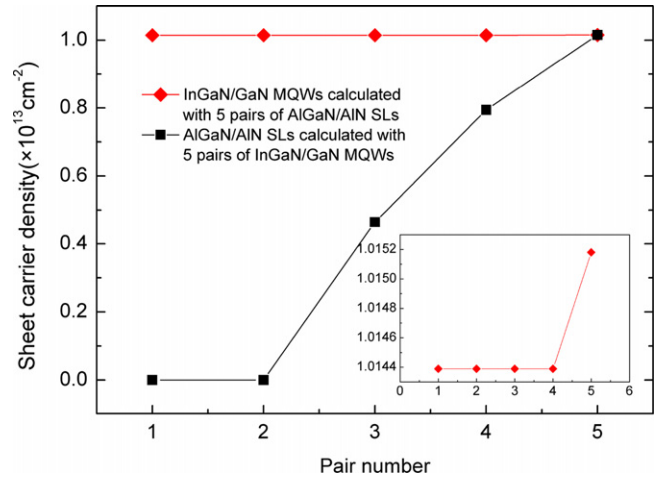

Fig. 5. Calculated sheet carrier density with different pairs of AlGaN/AlN SLs and InGaN/GaN MQWs. Inset: sheet carrier density versus different pairs of InGaN/GaN MQW with small scale.

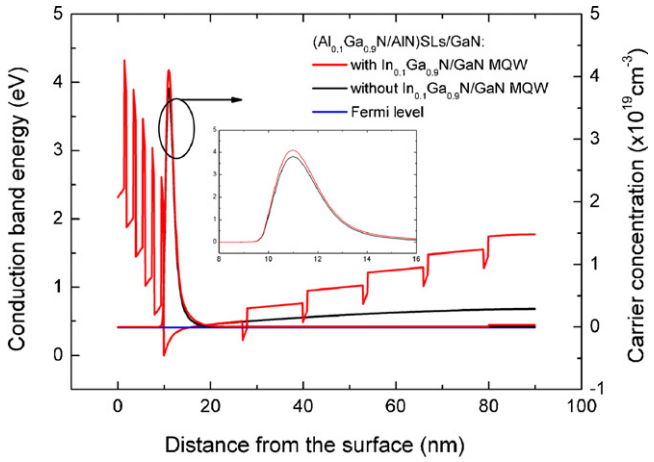

Fig. 7. Calculation of conduction band diagrams and carrier concentration distribution of $(Al_{0.1}Ga_{0.9}N/AlN)$SLs/GaN heterostructure with and without optimized $In_{0.1}Ga_{0.9}N$/GaN MQW, inset: a closer view of carrier concentration distribution.

increase of 2DEG density, and the corresponding carrier confinement characteristics can also be improved. However, a high tensile stress is expected to remain in the GaN channel layer due to the larger lattice constant of InGaN than GaN, and this lattice mismatch may deteriorate the quality of GaN channel leading to decrease of 2DEG density as well as mobility. Therefore, the pairs of InGaN/GaN MQWs are limited, and depending on the buffer layers below.

3.5. Electrical properties of 2DEG in optimized HEMT structure

In order to observe the effects of optimizations, a standard $(Al_{0.1}Ga_{0.9}N/AlN)$SLs/GaN structure without $In_{0.1}Ga_{0.9}N$/GaN MQW is chosen as a template and used for comparison at the end of the optimizations. The conduction band diagrams and carrier concentration distribution of $(Al_{0.1}Ga_{0.9}N/AlN)$SLs/GaN heterostructure with and without optimized $In_{0.1}Ga_{0.9}N$/GaN MQW are shown in Fig. 7. It can be seen that the carrier concentration increases from 3.87×10^{19} cm^{-3} to 4.1×10^{19} cm^{-3}. Nevertheless, the magnitude of the change is not significant, this is considered to be due to carriers mainly confined at the GaN channel and slightly spread over the barrier, and the contributions of InGaN layers to the total polarization field of HEMT structure is small. Actually, the carrier confinement of InGaN/GaN MQW back-barrier is more embodied in a dynamic process (operational state of device) such as preventing 2DEG leak to the buffer layer.

For $Al_yGa_{1-y}N$/AlN SLs barrier, the calculated Al composition dependence of the carrier ratio $R_{carrier}$ of $(Al_yGa_{1-y}N/AlN)$SLs/GaN/$(In_{0.1}Ga_{0.9}N/GaN)$MQW/GaN and standard AlGaN/GaN/$(In_{0.1}Ga_{0.9}N/GaN)$MQW/GaN heterostructure is shown in Fig. 8, $R_{carrier}$ is defined as follows:

$$R_{carrier} = \frac{n_{barrier}}{n_{HEMT}} \quad (7)$$

where $n_{barrier}$ is the carriers in the barrier lays, n_{HEMT} is the total carriers in HEMT. It is clear that the $R_{carrier}$ of both structures increases with the increase of Al composition. However, the $R_{carrier}$ of the designed heterostructure is much lower than that of conventional AlGaN/GaN/$(In_{0.1}Ga_{0.9}N/GaN)$MQW/GaN. This is considered to be due to the increase of conduction band offset ΔE_c and the strong polarization field at the interface between AlGaN/AlN SLs and GaN, and this dramatic decrease in $R_{carrier}$ indicates that the carrier penetration into barrier layer is greatly suppressed. Therefore, much stronger carrier confinement can be realized in the designed structure.

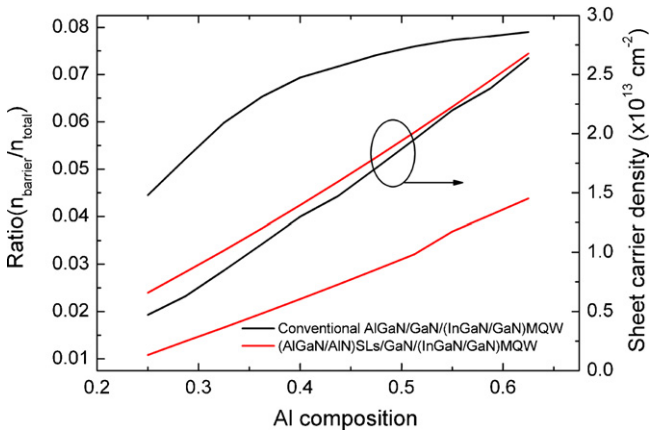

Fig. 8. Calculated Al composition dependence of the carrier ratio $R_{carrier}$ of $(Al_yGa_{1-y}N/AlN)$SLs/GaN/$(In_{0.1}Ga_{0.9}N/GaN)$MQW/GaN and conventional AlGaN/GaN/$(In_{0.1}Ga_{0.9}N/GaN)$MQW/GaN heterostructures.

Owing to the carrier confinement, the band profiles and carrier concentration distribution in designed heterostructure and conventional AlGaN/GaN structure with the Al composition being of 0.32 are shown in Fig. 9(a) and (b), respectively. It is clear that the 2DEG concentration increases from 3.24×10^{19} cm^{-3} to 4.1×10^{19} cm^{-3}, sheet carrier density increases from 8.472×10^{12} cm^{-2} to 1.015×10^{13} cm^{-2}, which is an increase of 19.8%. Furthermore, the distribution shifts to the right position

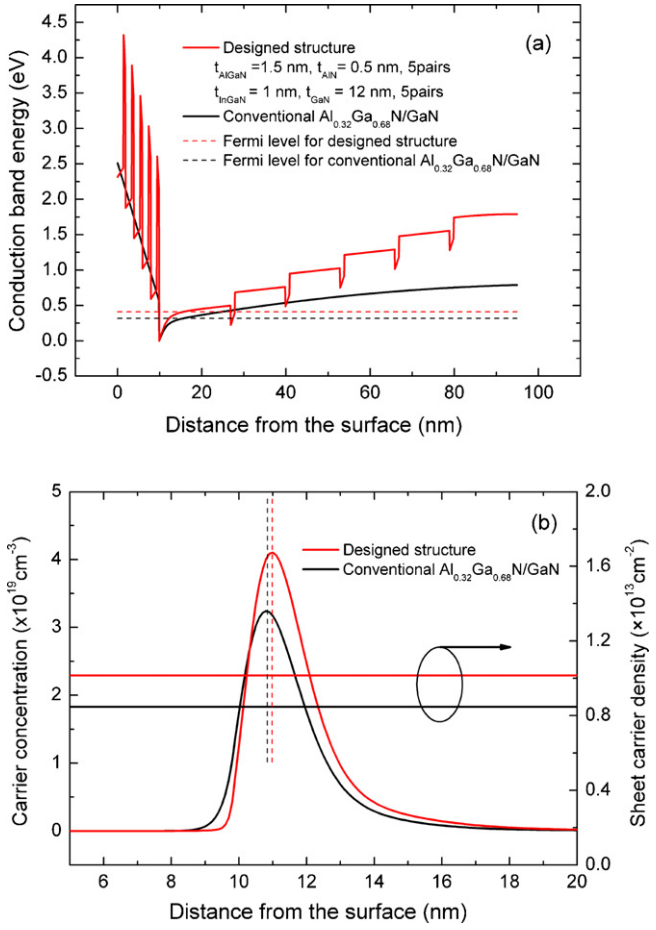

Fig. 9. (a) Calculated band profiles. (b) Carrier concentration distribution in designed heterostructure and conventional AlGaN/GaN structure with the Al composition being of 0.32.

further, where further away to the interface between AlGaN/AlN SLs and GaN channel. It is reported that the interface roughness will be the main scattering mechanism when 2DEG sheet carrier density was higher than 7×10^{12} cm^{-2} because the 2DEG distribution was further close to the heterointerface with the increase of 2DEG density [10]. Another short-range scattering mechanism, the alloy disorder scattering, will also strongly influence the transport properties of the 2DEG if its distribution is close to the heterointerface in AlGaN/GaN structure [27]. In our case, both interface roughness and alloy disorder scattering can be reduced, which indicate that the carrier mobility will be improved.

4. Conclusions

In this article, we have presented calculations of carrier confinement characteristics in ($Al_yGa_{1-y}N$/AlN)SLs/GaN/($In_xGa_{1-x}N$/GaN)MQW/GaN heterojunction structure in the presence of spontaneous and piezoelectrically induced polarization effects. The calculations were made using a self-consistent solution of the Schrödinger, Poisson, potential and charge balance equations. An optimization of $In_xGa_{1-x}N$/GaN MQW was made including thickness of GaN channel, InGaN, and indium composition of $In_xGa_{1-x}N$. According to the optimization results, thicknesses of 17 nm and 1 nm for the GaN channel layer and $In_{0.1}Ga_{0.9}N$ are proposed for high performance device with high 2DEG concentration and mobility.

In order to observe the effects of optimizations, a standard ($Al_{0.1}Ga_{0.9}N$/AlN)SLs/GaN structure without $In_{0.1}Ga_{0.9}N$/GaN MQW is chosen as a template and used for comparison at the end of the optimizations. It is found that carrier concentration and its distribution have no significant change, because carriers mainly confined at the GaN channel and the contribution of InGaN layers to the total polarization field of HEMT structure is small. Nevertheless, the carrier confinement of InGaN/GaN MQW back-barrier is expected to embody in the operational state of device. On the other hand, $R_{carrier}$ of the designed heterostructure is much lower than that of conventional AlGaN/GaN/($In_{0.1}Ga_{0.9}N$/GaN)MQW/GaN, which indicates that the $Al_yGa_{1-y}N$/AlN SLs barrier plays an important role in enhancing the confinement of the carrier.

Finally, the carrier concentration and its distribution in designed heterostructure and conventional AlGaN/GaN structure with the Al composition being of 0.32 were discussed. According to the calculations, a 19.8% increase in sheet carrier density is predicted for an optimized ($Al_{0.1}Ga_{0.9}N$/AlN)SLs/GaN/($In_{0.1}Ga_{0.9}N$/GaN)MQW/GaN structure compared to the conventional AlGaN/GaN one. Furthermore, the calculated carrier distribution indicates that the carrier mobility will be improved by reducing interface roughness and alloy disorder scattering in designed heterostructure. This simulation contributes to designing and fabricating high-performance GaN-based HEMTs.

Acknowledgments

This work has been supported by the Knowledge Innovation Engineering of Chinese Academy of Sciences (no. YYYJ-0701-02), the National Nature Sciences Foundation of China (nos. 60890193, 60906006), the State Key Development Program for Basic Research of China (nos. 2006CB604905, 2010CB327503), and the Knowledge Innovation Program of the Chinese Academy of Sciences (nos. ISCAS2008T01, ISCAS2009L01, ISCAS2009L02).

References

[1] S. Strite, H. Morkoc, J. Vac. Sci. Technol. B 10 (1992) 1237.
[2] I. Akasaki, S. Sota, H. Sakai, T. Tanaka, M. Koike, H. Amano, Electron. Lett. 32 (1996) 1105.
[3] E.S. Hellman, MRS Internet J. Nitride Semicond. Res. 3 (1998) 11.
[4] X.L. Wang, C.M. Wang, G.X. Hu, J.X. Ran, J.X. Wang, T.S. Chen, G. Jiao, J.P. Li, Y.P. Zeng, J.M. Li, Solid State Electron. 49 (8) (2005) 1387.
[5] M. Miyoshi, H. Ishikawa, T. Egawa, K. Asai, M. Mouri, T. Shibata, M. Tanaka, O. Oda, Appl. Phys. Lett. 85 (2004) 1710.
[6] Y.F. Wu, A. Saxler, M. Moore, R.P. Smith, S. Sheppard, P.M. Chavarkar, T. Wisleder, U.K. Mishra, P. Parikh, IEEE Electron. Device Lett. 25 (2004) 117.
[7] M. Asif Khan, Q. Chen, M.S. Shur, B.T. Mcdermott, J.A. Higgins, J. Burm, W.J. Schaff, L.F. Eastman, IEEE Electron Device Lett. 17 (1996) 584.
[8] O. Ambacher, J. Smart, J.R. Shealy, N.G. Weimann, K. Chu, M. Murphy, W.J. Schaff, L.F. Eastman, R. Dimitrov, L. Wittmer, M. Stutzmann, W. Rieger, J. Hilsenbeck, J. Appl. Phys. 85 (1999) 3222.
[9] P.M. Asbeck, E.T. Yu, S.S. Lau, G.J. Sullivan, J.V. Hove, J. Redwing, Electron. Lett. 33 (1997) 1240.
[10] J. Antoszewski, M. Gracey, J.M. Dell, L. Faraone, T.A. Fisher, G. Parish, Y.F. Wu, U.K. Mishra, J. Appl. Phys. 87 (2000) 3900.
[11] C.Q. Chen, J.P. Zhang, V. Adivarahan, A. Koudymov, Appl. Phys. Lett. 82 (25) (2003) 4593–4595.
[12] G. Simin, A. Koudymov, H. Fatima, IEEE Electron Device Lett. 23 (8) (2002) 458–460.
[13] M. Micovic, P. Hashimoto, Hu Ming, I. Milosavljevic, J. Duvall, P.J. Willadsen, W.S. Wong, A.M. Conway, A. Kurdoghlian, P.W. Deelman, M. Jeong, S.A. Schmitz, M.J. Delaney, IEDM Tech. Dig. (2004) 807–810.
[14] Y. Kawakami, A. Nakajima, X.Q. Shen, G. Piao, M. Shimizu, H. Okumura, Appl. Phys. Lett. 90 (2007) 242112.
[15] K.H. Lee, P.C. Chang, S.J. Chang, Y.K. Su, C.L. Yu, Appl. Phys. Lett. 96 (2007) 212105.
[16] B. Jogai, J. Appl. Phys. 93 (2003) 1631.
[17] Asbeck, P.M. Yu, E.T. Lau, S.S. Sullivan, G.J. Hove, Van Hove, J. Redwing, J. Electron. Lett. 33 (1997) 1230.
[18] F. Bernardinin, V. Fiorentini, D. Vanderbilt, Phys. Rev. B 56 (1997) R10024.
[19] O. Ambacher, B. Foutz, J. Smart, J.R. Shealy, N.G. Weimann, K. Chu, M. Murphy, A.J. Sierakowski, W.J. Schaff, L.F. Eastman, R. Dimitrov, A. Mitchell, M. Stutzmann, J. Appl. Phys. 87 (2000) 334.
[20] V.M. Bermudez, C.I. Wu, A. Khan, J. Appl. Phys. 89 (2001) 1991.
[21] R.Y. Korotkov, J.M. Gregie, B.W. Wessels, Appl. Phys. Lett. 80 (2002) 1731.
[22] H. Okumura, Jpn. J. Appl. Phys. Part 1 45 (2006) 7565.
[23] L.C. Guo, X.L. Wang, H.L. Xiao, B.Z. Wang, J. Cryst. Growth 298 (2007) 522.
[24] J. Liberis, I. Matulioniene, A. Matulionis, E. Šermukšnis, J. Xie, J.H. Leach, H. Morkoc, Phys. Status Solidi (a) 206 (2009) 1385.
[25] R. Vetury, N.Q. Zhang, S. Keller, U.K. Mishra, IEEE Trans. Electron Devices 48 (2001) 560–566.
[26] A.M. Wells, M.J. Uren, R.S. Balmer, K.P. Hilton, T. Martin, M. Missous, Solid-State Electron. 49 (2005) 279–282.
[27] L. Hsu, W. Walukiewicz, Phys. Rev. B 56 (1997) 1520.